AGU PUBLICATIONS

JGR

Journal of Geophysical Research: Space Physics

RESEARCH ARTICLE
10.1002/2014JA020877

Special Section:
Big Storms of the Van Allen Probes Era

Van Allen Probes, THEMIS, GOES, and Cluster observations of EMIC waves, ULF pulsations, and an electron flux dropout

K. Sigsbee[1], C. A. Kletzing[1], C. W. Smith[2], R. MacDowall[3], H. Spence[2], G. Reeves[4], J. B. Blake[5], D. N. Baker[6], J. C. Green[7], H. J. Singer[8], C. Carr[9], and O. Santolík[10,11]

[1]Department of Physics and Astronomy, University of Iowa, Iowa City, Iowa, USA, [2]Institute for Earth, Oceans and Space, University of New Hampshire, Durham, New Hampshire, USA, [3]Planetary Magnetospheres Laboratory, NASA Goddard Space Flight Center, Greenbelt, Maryland, USA, [4]Space and Atmospheric Sciences, NIS-1, Los Alamos National Laboratory, Los Alamos, New Mexico, USA, [5]Aerospace Corporation, El Segundo, California, USA, [6]Laboratory for Atmospheric and Space Physics, University of Colorado Boulder, Boulder, Colorado, USA, [7]Space Hazards Applications, Golden, Colorado, USA, [8]Space Weather Prediction Center, National Oceanic and Atmospheric Administration, Boulder, Colorado, USA, [9]Department of Physics, Imperial College, London, UK, [10]Institute of Atmospheric Physics AS CR, Prague, Czech Republic, [11]Faculty of Mathematics and Physics, Charles University in Prague, Prague, Czech Republic

Key Points:
- Data from seven spacecraft were analyzed during the 12-14 November 2012 storm
- EMIC waves were observed by five spacecraft during an electron flux dropout
- Both adiabatic and nonadiabatic processes needed to explain electron losses

Correspondence to:
K. Sigsbee,
kristine-sigsbee@uiowa.edu

Citation:
Sigsbee, K., et al. (2016), Van Allen Probes, THEMIS, GOES, and Cluster observations of EMIC waves, ULF pulsations, and an electron flux dropout, *J. Geophys. Res. Space Physics*, *121*, 1990–2008, doi:10.1002/2014JA020877.

Received 21 NOV 2014
Accepted 22 JAN 2016
Accepted article online 28 JAN 2016
Published online 4 MAR 2016

Abstract We examined an electron flux dropout during the 12–14 November 2012 geomagnetic storm using observations from seven spacecraft: the two Van Allen Probes, Time History of Events and Macroscale Interactions during Substorms (THEMIS)-A (P5), Cluster 2, and Geostationary Operational Environmental Satellites (GOES) 13, 14, and 15. The electron fluxes for energies greater than 2.0 MeV observed by GOES 13, 14, and 15 at geosynchronous orbit and by the Van Allen Probes remained at or near instrumental background levels for more than 24 h from 12 to 14 November. For energies of 0.8 MeV, the GOES satellites observed two shorter intervals of reduced electron fluxes. The first interval of reduced 0.8 MeV electron fluxes on 12–13 November was associated with an interplanetary shock and a sudden impulse. Cluster, THEMIS, and GOES observed intense He^+ electromagnetic ion cyclotron (EMIC) waves from just inside geosynchronous orbit out to the magnetopause across the dayside to the dusk flank. The second interval of reduced 0.8 MeV electron fluxes on 13–14 November was associated with a solar sector boundary crossing and development of a geomagnetic storm with $Dst < -100$ nT. At the start of the recovery phase, both the 0.8 and 2.0 MeV electron fluxes finally returned to near prestorm values, possibly in response to strong ultralow frequency (ULF) waves observed by the Van Allen Probes near dawn. A combination of adiabatic effects, losses to the magnetopause, scattering by EMIC waves, and acceleration by ULF waves can explain the observed electron behavior.

1. Introduction

The Earth's radiation belt environment exhibits a high degree of variability due to both adiabatic and nonadiabatic processes that can swiftly alter particle fluxes. Indeed, many studies have noted that radiation belt electron fluxes can increase, decrease, or even remain the same in response to geomagnetic storms and that this response can appear to be independent of *L* shell or the strength of the storm [e.g., *Reeves*, 1998; *Reeves et al.*, 2003]. Under the right conditions, the fluxes of outer radiation belt electrons with energies from a few tens of keV up to several MeV can "dropout" or rapidly decrease by one or more orders of magnitude over a broad range of *L* shells due to adiabatic effects and permanent losses to the magnetopause and ionosphere [e.g., *Onsager et al.*, 2002; *Millan and Thorne*, 2007; *Bortnik et al.*, 2006; *Turner et al.*, 2013]. Although electron flux dropouts have typically been associated with the storm main phase, they have also been observed independently of geomagnetic storms [*Morley et al.*, 2010].

The "*Dst* effect," in which the development of the storm time ring current and associated decrease of the inner magnetosphere magnetic field strength cause an observed decrease in the energetic electron fluxes [*Li et al.*, 1997; *Kim and Chan*, 1997], is an example of an adiabatic, reversible process that can explain electron flux dropouts. As its name suggests, the key indicator of this effect is a strong correlation between decreases in the energetic electron fluxes and the decrease in the *Dst* index during the storm main phase. Stretching of the magnetic fields due to the formation of a partial ring current near dusk [e.g., *Onsager et al.*, 2002; *Green et al.*, 2004] can also produce a localized electron loss due to changes in the magnetic field topology. Since the electron fluxes do not always immediately

return to pre-event levels after dropouts, irreversible, nonadiabatic processes causing permanent losses of electrons may also be involved. "Magnetopause shadowing" on the dayside can cause depletions of the electron fluxes when particle drift paths cross the magnetopause and are lost from the magnetosphere [*West et al*., 1972]. Strong, southward interplanetary magnetic field (IMF) and increases in the solar wind dynamic pressure can cause the last closed drift shell in the dayside magnetosphere to move earthward, resulting in permanent electron losses from the outer regions of the radiation belts [e.g., *Kim et al*., 2008, 2010; *Matsumura et al*., 2011; *Yu et al*., 2013]. Outward radial transport can also contribute to losses to the magnetopause [*Turner et al*., 2012].

Wave-particle interactions with electromagnetic ion cyclotron (EMIC) waves can induce rapid electron scattering [*Thorne and Kennel*, 1971] and may also contribute to permanent losses of relativistic electrons during the storm main phase [*Li et al*., 1997]. EMIC waves propagate in three bands below the proton gyrofrequency: a hydrogen band between the He^+ and H^+ gyrofrequencies, a helium band between the O^+ and He^+ gyrofrequencies, and an oxygen band below the O^+ gyrofrequency. Ion composition and anisotropy [*Kozyra et al*., 1984; *Thorne and Horne*, 1994], along with geomagnetic activity levels [*Bräysy et al*., 1998] influence which bands are excited. EMIC waves have traditionally been thought of as transverse, left-hand polarized magnetic field fluctuations. However, right-hand and linearly polarized EMIC waves have been observed [*Anderson et al*., 1992a; *Min et al*., 2012; *Paulson et al*., 2014; *Allen et al*., 2015]. Also, some published EMIC wave examples have weak parallel components, and statistical results indicate that propagation at large wave normal angles is possible [*Anderson et al*., 1992a, 1992b; *Min et al*., 2012; *Allen et al*., 2015]. EMIC waves affect only relativistic electrons as the resonant energies for wave-particle interactions with these waves are typically above 0.5 MeV [e.g., *Meredith et al*., 2003].

Combinations of adiabatic effects and permanent losses due to magnetopause shadowing and EMIC waves are often responsible for the observed electron behavior. For example, *Bortnik et al*. [2006] studied an electron dropout event on 20 November 2003 and found that the behavior of the electrons varied across L shells. For $L > 5$, *Bortnik et al*. [2006] found that the dropout was approximately independent of energy and was consistent with losses to the magnetopause assisted by the *Dst* effect and outward radial diffusion. For $L < 5$, the dropout was energy dependent and consistent with pitch angle scattering by EMIC waves.

In this paper, we present Van Allen Probes (formerly known as the Radiation Belt Storm Probes, RBSP-A and RBSP-B), Time History of Events and Macroscale Interactions during Substorms (THEMIS), Geostationary Operational Environmental Satellite (GOES), and Cluster observations during an electron flux dropout that occurred during the 12–14 November 2012 geomagnetic storm. We will use the geomagnetic indices and solar wind parameters in the NASA OMNI data set [*King and Papitashvili*, 2005] to examine the upstream drivers of this storm and to determine the sequence of the wave and particle observations in the overall evolution of the storm. During the time period of interest, solar wind flow speeds and magnetic fields were available from both Wind and the Advanced Composition Explorer (ACE) near L1. However, densities were only available from Wind, so NASA OMNI data for this event are based mainly upon Wind data propagated to the Earth's bow shock nose. Using THEMIS, GOES, and Cluster data, we will discuss the spatial extent of EMIC waves observed on 12–14 November 2012. Electron data from the Van Allen Probes and GOES satellites will be used to examine the development of the flux dropout. We will also examine ULF waves in the Pc4 and Pc5 bands observed by the Van Allen Probes and GOES satellites during this event.

2. Start of the Electron Dropout on 12 November Before the Shock Arrival

According to the NOAA Space Weather Prediction Center Preliminary Reports and Forecasts of Solar Geophysical Data issued for 5–11 November 2012 and 12–18 November 2012, the geomagnetic activity on 12–14 November was related to two earthward directed coronal mass ejections (CMEs). The first CME was observed on 9 November at 1524 UT in the Solar and Heliospheric Observatory (SOHO) Large Angle and Spectroscopic Coronagraph (LASCO) C2 images [*Brueckner et al*., 1995] and the second on 10 November in Solar Terrestrial Relations Observatory (STEREO) A COR2 coronagraph images [*Howard et al*., 2008] at 0504 UT and SOHO/LASCO C3 images at 1054 UT.

Figure 1 shows an overview of the geomagnetic activity and OMNI solar wind parameters at the Earth's bow shock nose, electron data from GOES and the Van Allen Probes, the *Dst* index, and the *Kp* index during the 72 h period starting at 0000 UT on 12 November 2012 and ending at 0000 UT on 15 November 2012. Changes in the solar wind ahead of the shock associated with the CMEs began priming the magnetosphere for the development of an electron flux dropout. For the first half of 12 November, the solar wind speed was

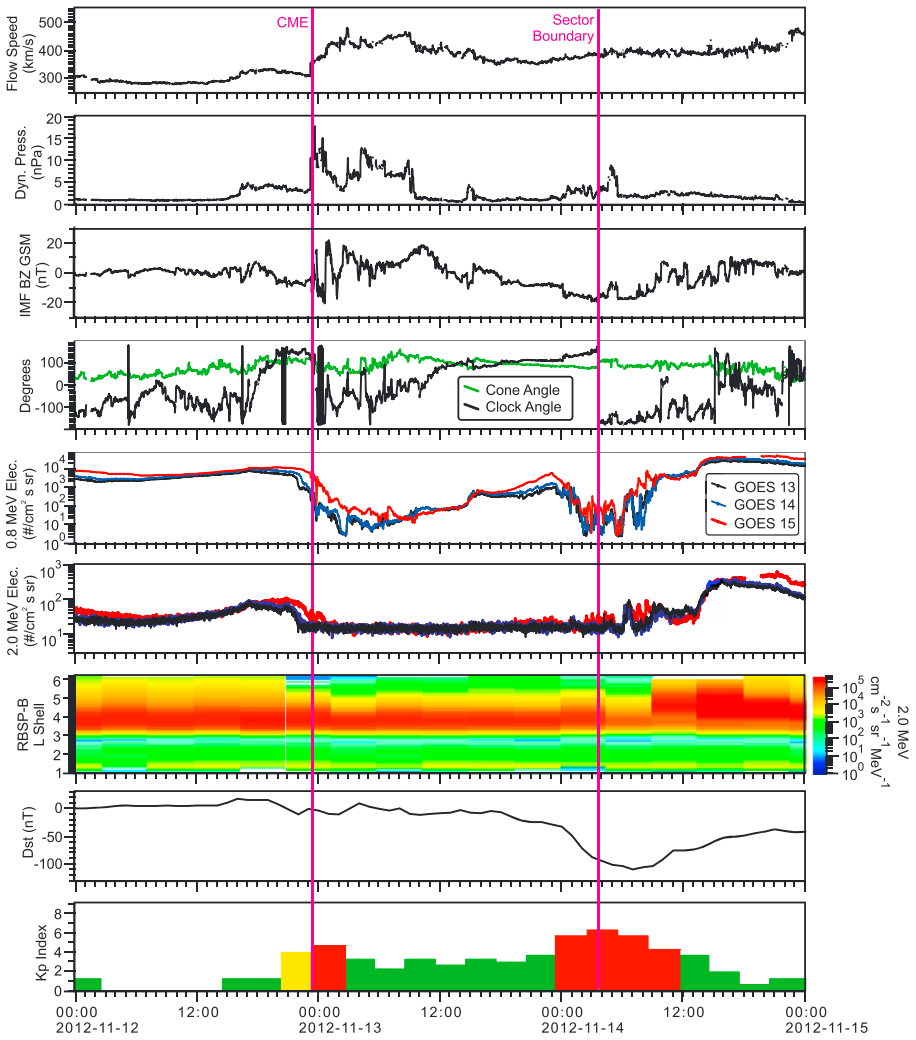

Figure 1. An overview of the geomagnetic activity on 12–14 November 2012. (first–fourth panels) OMNI solar wind flow speed, dynamic pressure, interplanetary magnetic field (IMF) B_z in GSM coordinates, and the solar wind clock and cone angles. All OMNI parameters have been propagated to the Earth's bow shock. (fifth and sixth panels) The 0.8 MeV and 2.0 MeV electron fluxes measured by GOES 13, 14, and 15. (seventh–ninth panels) The Relativistic Electron-Proton Telescope (REPT) electrons for energies of 2.0 MeV from Van Allen Probe B (RBSP-B) as a function of *L* shell and time, the *Dst* index, and the *Kp* index. The times of the shock arrival on 12 November at 2316 UT and the time of the solar wind sector boundary on 14 November at 0336 UT have been marked with magenta lines.

very low at both Wind and ACE, with typical values around 280 km/s, and the solar wind B_z GSM was fluctuating around 0 nT. After 1200 UT, the solar wind speed began to increase gradually. A sudden increase in the Wind proton density from ~11 cm^{-3} to 17 cm^{-3} around 1500 UT combined with the increasing solar wind speeds resulted in a jump in the OMNI dynamic pressure from 2 nPa to 4.5 nPa at the bow shock about an hour later at 1600 UT. At about 1800 UT, the B_z GSM component of the interplanetary magnetic field measured by Wind and ACE turned southward ahead of the CME shock.

Figure 2 shows the portions of the GOES, THEMIS A, and Cluster 2 orbits when EMIC waves were observed on 12–13 November as a function of *L* and magnetic local time. EMIC waves were observed by GOES 14 and 15 for the longest time period of all five spacecraft, between 12 November 1610 UT and 13 November 1000 UT. GOES 13, THEMIS, and Cluster observed EMIC waves for shorter intervals within this time period. In order to examine the EMIC waves and ULF pulsations, we transformed the magnetic field data from these spacecraft into a field-aligned coordinate system commonly used for studying the polarization of low-frequency waves [e.g., *Anderson*, 1994; *Eriksson et al.*, 2005]. We took a 30 min running magnetic field average to obtain the measured background magnetic field and subtracted

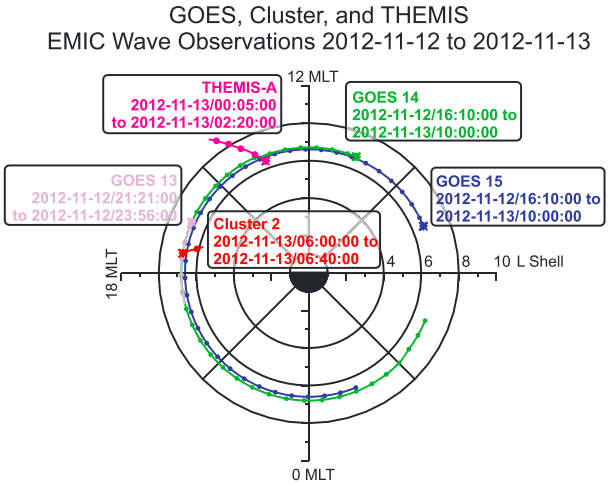

Figure 2. The portions of the orbits of GOES 13, 14, and 15, THEMIS, and Cluster 2 when EMIC waves were observed on 12–13 November as a function of *L* shell and MLT. The start of each trajectory is marked with a star, and dots are placed for every hour and 30 min after the hour.

this background magnetic field from the total magnetic field to obtain the residual wave magnetic fields. The background magnetic field direction defines the parallel unit vector $\hat{\boldsymbol{p}}$ in our field-aligned coordinate system. The two components perpendicular to the background magnetic field are chosen, so

$$\hat{\boldsymbol{e}} = [\hat{\boldsymbol{p}} \times \boldsymbol{R}]/|\hat{\boldsymbol{p}} \times \boldsymbol{R}|$$

gives the eastward direction, where $\boldsymbol{R}$ is the radius vector of the satellite, and

$$\hat{\boldsymbol{r}} = \hat{\boldsymbol{e}} \times \hat{\boldsymbol{p}}$$

is meridional or radially outward at the magnetic equator. This field-aligned coordinate system can be used to determine the polarizations of ULF pulsations. ULF waves that appear primarily in the spectrograms of the $\hat{\boldsymbol{p}}$ component, which is parallel to the background magnetic field, are compressional. Waves that appear primarily in the radial $\hat{\boldsymbol{r}}$ component are poloidal waves, and waves that appear primarily in the azimuthal or eastward $\hat{\boldsymbol{e}}$ component are toroidal waves [e.g., *Hughes*, 1994].

Figure 3 (first–third panels) shows spectrograms made by performing a fast Fourier transform (FFT) with a sliding Hanning window on the GOES 15 wave magnetic fields in the field-aligned coordinate system

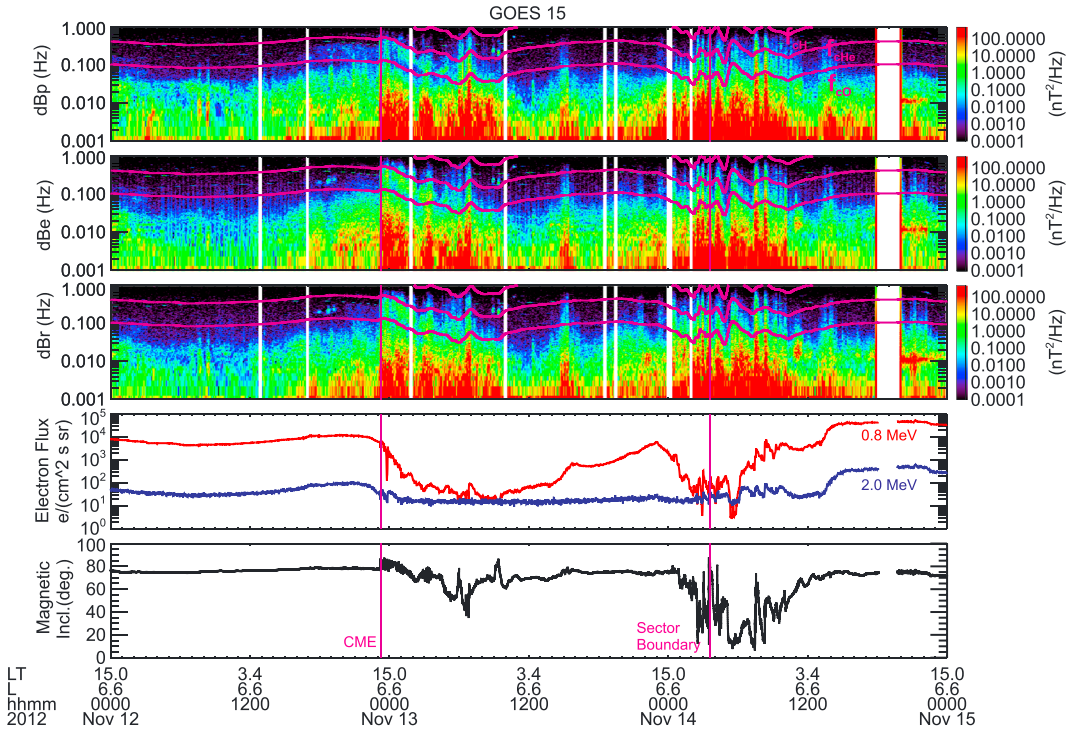

Figure 3. (first–third panels) FFT spectrograms of the GOES 15 parallel (dBp), eastward (dBe), and radial (dBr) wave magnetic fields. Magenta lines for the O^+, He^+, and H^+ ion gyrofrequencies have been overplotted on the spectrograms. (fourth and fifth panels) The 0.8 and 2.0 MeV electron fluxes and the magnetic field inclination angle at GOES 15. The times of the shock arrival on 12 November at 2316 UT and the solar wind sector boundary crossing on 14 November at 0336 UT have been marked with a vertical magenta line.

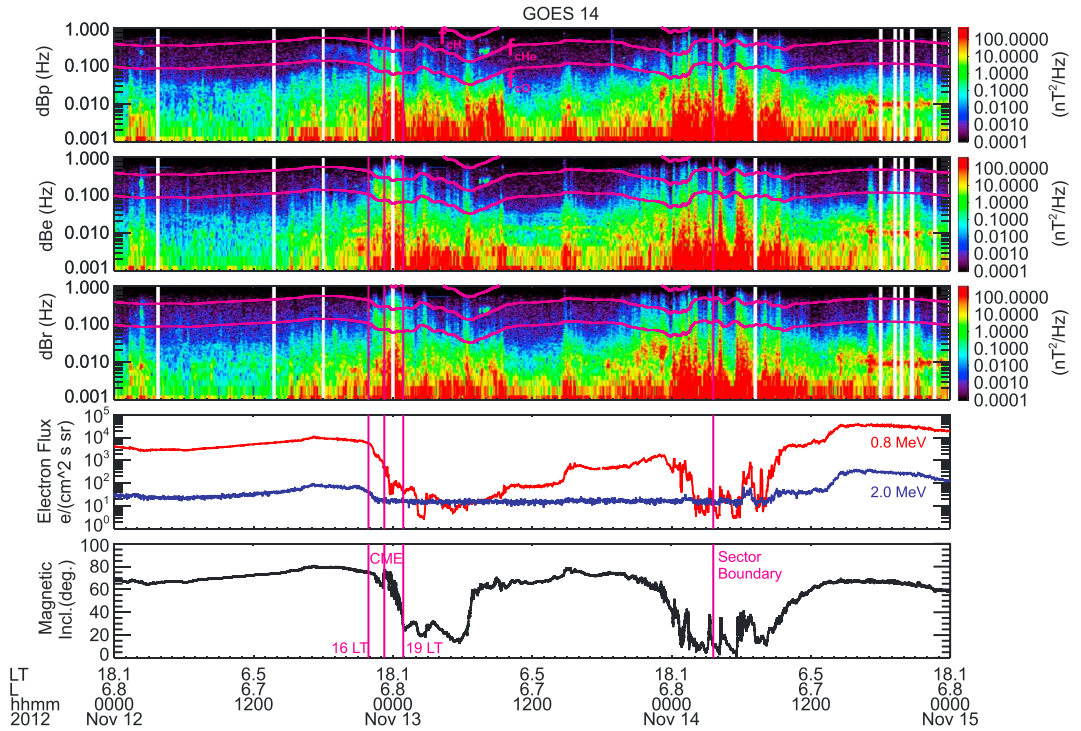

Figure 4. FFT spectrograms of the GOES 14 wave magnetic fields in field-aligned coordinates and GOES 14 electron fluxes. The format is the same as Figure 3. The times at which GOES 14 was located at 16 LT and 19 LT have also been marked with vertical magenta lines.

described above for the same 72 h period from 0000 UT on 12 November 2012 to 0000 UT on 15 November 2012 shown in Figure 1. Figure 3 (fourth and fifth panels) shows the 0.8 and 2.0 MeV electron fluxes and the magnetic field inclination to the orbital plane for GOES 15. Magenta lines for the O^+, He^+, and H^+ ion gyrofrequencies have been overplotted on the spectrograms. Shortly after the increase in solar wind dynamic pressure at the bow shock around 1600 UT, very weak magnetic field fluctuations in the He^+ EMIC wave bands began to be recorded on the dayside at geosynchronous orbit by GOES 15 on 12 November around 1610 UT near 7.3 LT, as shown in Figure 3. Figure 4 shows data from the same 72 h period as Figure 3 for GOES 14, which also began observing very weak fluctuations in the He^+ EMIC band around 1610 UT, near 10.3 LT. This suggests that EMIC waves may have been excited over a broad range of local times on the dayside at geosynchronous orbit by the slight increase in solar wind dynamic pressure near 1600 UT. Figure 5 shows GOES 13 data from the same 72 h period as Figures 1, 3, and 4. Figure 5 shows that GOES 13 began observing intense EMIC waves on 12 November starting at 2121 UT when the satellite was located near 16 LT and continuing until 2356 UT when the satellite was located near 19 LT. GOES 14 also saw an increase in the intensity of the EMIC waves starting at 2157 UT when the spacecraft had moved to 16 LT that lasted until 0048 UT on 13 November when the spacecraft was located near 19 LT. The increases in the EMIC wave intensity recorded by GOES 13 and GOES 14 on the dusk flank of the magnetosphere were most likely caused by these two satellites moving into a region of stronger wave activity near 16–19 LT.

ULF waves in the Pc4 (7–22 mHz) and Pc5 (2–7 mHz) bands [*Jacobs et al.*, 1964] were also observed by the GOES satellites throughout the entire time period shown in Figures 3, 4, and 5, with increased wave amplitudes during intervals of enhanced solar wind drivers. Figure 6 shows FFT spectrograms of wave magnetic fields from the Electric and Magnetic Field Instrument Suite and Integrated Science (EMFISIS) [*Kletzing et al.*, 2013] in field-aligned coordinates for Van Allen Probe B (RBSP-B) for the same 72 h time period shown in Figures 1, 3, 4, and 5. During the time period of interest, the apogees of the Van Allen Probes were located near dawn. Data from several orbits are shown in Figure 6. Both Van Allen Probes observed strong ULF waves throughout the electron dropout and subsequent geomagnetic storm. Compressional Pc4 pulsations were observed by the Van Allen Probes before noon on 12 November, as shown by the band near 0.01 Hz in the

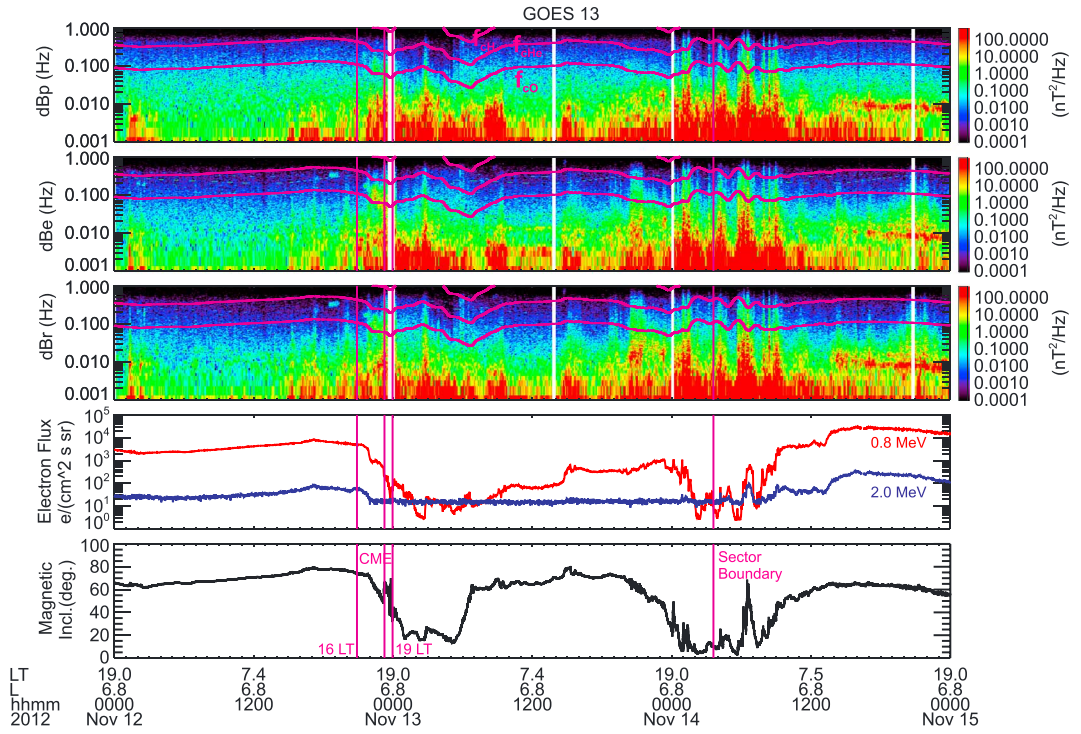

Figure 5. FFT spectrograms of the GOES 13 wave magnetic fields in field-aligned coordinates and GOES 13 electron fluxes. The format is the same as Figures 3 and 4. The times at which GOES 13 was located at 16 LT and 19 LT have been marked with vertical magenta lines.

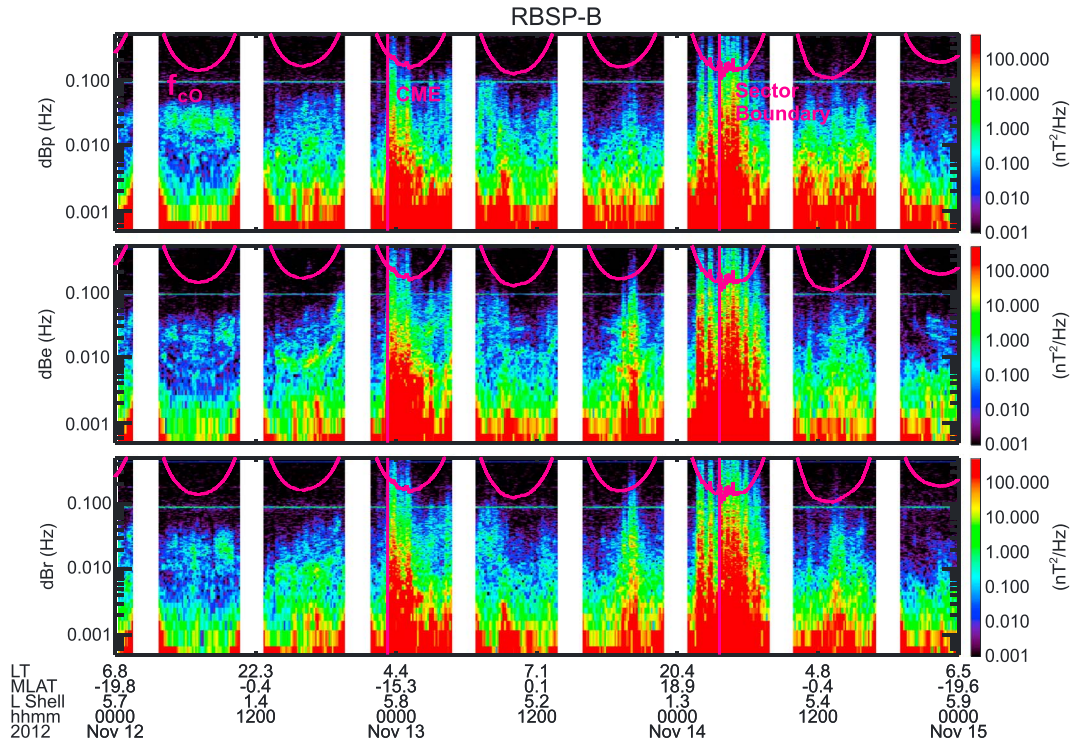

Figure 6. FFT spectrograms of the Van Allen Probe B (RBSP-B) wave magnetic fields in field-aligned coordinates showing ULF wave observations for 12–14 November. A magenta line for the O^+ ion gyrofrequency has been overplotted on the spectrograms.

parallel component of the magnetic field. Lower frequency compressional waves in the Pc5 frequency range were also observed. Toroidal field line resonances and harmonics were observed in the Pc4–Pc5 frequency ranges as shown by the eastward component of the magnetic field on 12 November. These are similar to the multiharmonic toroidal standing Alfvén waves reported in Van Allen Probes data from a few days earlier on 8 November 2012 [*Takahashi et al*., 2015]. Consistent with *Takahashi et al*. [2015], the toroidal harmonics observed during the time period shown in Figure 6 generally appear to have larger amplitudes when the IMF cone angle shown in Figure 1 is smaller.

Figures 3–5 (fourth and fifth panels) show the 0.8 and 2.0 MeV electron fluxes measured by the Energetic Proton, Electron, and Alpha Detector (EPEAD) electron detectors on GOES 13, 14, and 15, as well as the magnetic field inclinations relative to the orbital plane. The standard coordinate system used for GOES magnetic field data is the PEN coordinate system, where the *P* component is perpendicular to the orbital plane and parallel to the Earth's spin axis, the *E* component is directed earthward in the orbital plane, and the *N* component is perpendicular to the other two components, pointing eastward. Note that *P* and *E* in this coordinate system are not the same as $\hat{\boldsymbol{p}}$ (parallel) and $\hat{\boldsymbol{e}}$ (eastward) in the field-aligned coordinate system. In this coordinate system, the magnetic field inclination angle relative to the orbital plane can be defined as

$$\theta = \tan^{-1}\left(\frac{B_P}{\sqrt{B_E{}^2 + B_N{}^2}}\right).$$

High magnetic field inclinations close to 90° imply a more dipolar magnetic field, while low magnetic field inclinations close to 0° suggest a stretched, tail-like magnetic field. In this paper, the magnetic field inclination is used to determine if the observed electron flux variations are most likely caused by reversible magnetic field changes due to the formation of a partial ring current [e.g., *Onsager et al*., 2002; *Green et al*., 2004], as well as the *Dst* effect [*Li et al*., 1997; *Kim and Chan*, 1997]. In the radiation belts, the observation of low magnetic field inclinations relative to the orbital plane and tail-like magnetic fields can be interpreted as an indication that the particle trapping boundary may be located earthward of the satellite [e.g., *Onsager et al*., 2002]. However, this does not necessarily mean that the particles have been lost, only that their trajectories have been altered. Note that the decreases in magnetic field configuration associated with the storm time development of a partial ring current near dusk and the *Dst* effect, as well as the effects of enhanced solar wind convection on the magnetotail seen on the nightside, are large-scale features that persist for several hours UT and are observed while the GOES spacecraft move through several hours in magnetic local time. On the nightside, shorter duration increases in the magnetic field inclination can be superimposed on top of the large-scale decreases in inclination associated with the geomagnetic storm. These shorter duration inclination changes on the nightside are likely related to substorm activity and the passage of dipolarization fronts over the spacecraft [e.g., *Sigsbee et al*., 2005; *Lopez et al*., 1988]. As the main goal of this paper is to understand the electron behavior over a 72 h period during a storm in November 2012, we are concerned primarily with changes in magnetic field orientation lasting more than several hours associated with the ring current and convection, and not the short-time scale fluctuations produced by substorm activity. It should be noted that for both the longer time scale magnetic field changes associated with the storm and the shorter time scale dipolarization fronts, high magnetic inclination angles mean only that the geomagnetic field assumes a more dipole-like configuration and are not meant to suggest that the field has actually become dipolar.

The 0.8 MeV and 2.0 MeV electron fluxes observed by GOES 13 and GOES 14 were gradually increasing at the start of 12 November 2012. During the time period of increasing electron fluxes on 12 November, the magnetic fields at GOES 13 and 14 were highly dipolar. The 2 MeV electron flux measured reached its maximum value at GOES 14 at 1709 UT and at GOES 13 a few minutes later at 1713 UT on 12 November. The 2 MeV electron flux observed by GOES 13 began to decrease after reaching its peak value at 1713 UT, so that it had already reached instrumental background levels by 2201 UT, more than an hour before the shock arrival and sudden impulse at 2316 UT. The 2 MeV electron flux at GOES 14 began to decrease after its peak value at 1709 UT, until it reached instrumental background levels at 2230 UT, also well before the shock arrival.

The GOES 13 and GOES 14 0.8 MeV electron fluxes reached their peak values on 12 November at 1713 UT, simultaneously with the 2 MeV electrons at GOES 13. After reaching peak values on 12 November, the

0.8 MeV electron fluxes observed by all three GOES spacecraft began to decrease throughout the rest of the day but did not reach their minimum values until after the shock arrival on 13 November. At first, the 0.8 MeV electron fluxes at GOES 13 and 14 decreased gradually. However, when the magnetic field at these two satellites started to become more stretched, the 0.8 MeV electron fluxes began to decrease rapidly. The magnetic field inclination at GOES 13 was consistently above 70° until 2154 UT on 12 November, when GOES 13 was located near 16.9 LT. After this time the magnetic field inclination began to decrease over the next 4 h, dropping to about 17° by 0100 UT on 13 November, when GOES 13 was located at 20 LT. At GOES 14, the magnetic field inclination remained consistently above 60°–70° until about 2200 UT on 12 November, when GOES 14 was located near 16.4 LT. After this time, the magnetic field inclination at GOES 14 dropped steeply until 0105 UT on 13 November, when GOES 14 was located near 19.2 LT. The highly stretched magnetic fields observed by GOES 13 and 14 near dusk are likely related to development of a partial ring current.

The behavior of the magnetic fields and electron fluxes at GOES 13 and 14 was similar, most likely due to the proximity of these two satellites in local time. The changes in the magnetic configuration and timing of the electron flux decreases were different at GOES 15, which is separated from GOES 13 and 14 by a few hours in local time and is located about 5° lower in magnetic latitude than GOES 13 and 14. Just like at GOES 13 and 14, the 0.8 MeV and 2.0 MeV electron fluxes observed at GOES 15 gradually increased from the start of 12 November 2012. However, the 2 MeV electron flux observed by GOES 15 did not reach its maximum value on 12 November until very late in the day at 2054 UT. The magnetic field inclination at GOES 15 was close to 75° from 0000 UT on 12 November up to the time of the shock arrival at 2316 UT on 12 November. This is rather interesting as GOES 15 was located on the dayside near 15 LT at 0000 UT, passed through midnight at 0833 UT, and reached 6 LT at 1442 UT, indicating that GOES 15 observed somewhat dipolar fields all across the nightside on 12 November. The 2 MeV electron flux at GOES 15 decreased after reaching its peak value on 12 November but did not reach instrumental background levels until after the start of 13 November. The 0.8 MeV electron flux did not reach its peak value at GOES 15 until 1950 UT on 12 November, much later than at GOES 13 and 14. The 0.8 MeV electron flux peak at GOES 15 occurred about an hour before the 2.0 MeV peak, unlike at GOES 13 and 14 where the 0.8 and 2.0 MeV fluxes peaked around the same time. After reaching peak values on 12 November, the 0.8 MeV electron fluxes observed by GOES 15 decreased throughout the rest of the day but did not reach their minimum values until after the shock arrival on 13 November.

The initial development of the electron dropout on 12 November appears reasonably well correlated with the development of stretched magnetic fields near dusk and the start of EMIC waves at geosynchronous orbit. The two satellites closest to dusk, GOES 13 and 14, observed the start of the electron dropout first, while GOES 15, which was located at earlier local times observed the start of the dropout after GOES 13 and 14. The relative timing of the start of the electron dropout at GOES 13, 14, and 15 is likely related to the observed differences in the local magnetic field configurations near noon and on the dusk flank and the drifts of the electrons through these different fields.

3. Shock Arrival and Continuation of the Electron Dropout on 13 November 2012

The shock associated with the CMEs arrived at ACE on 12 November 2216 UT and was followed by the observation of a 16 nT sudden impulse by the Boulder U.S. Geological Survey magnetometer an hour later at 2316 UT. The maximum southward IMF B_z reached was −19.5 nT at 2338 UT, and the total IMF reached a maximum value of 22.8 nT on 13 November at 0053 UT. The solar wind speed measured by ACE peaked at 504 km/s at 0111 UT on 13 November. Geomagnetic activity levels were unsettled to active throughout 13 November due to the shock arrival, as indicated by the increase in the *Kp* index. EMIC waves continued to be observed by GOES 13, 14, and 15 after the shock arrival and were also observed by Cluster and THEMIS on 13 November. The Van Allen Probes observed bursty, broadband ULF waves around the time of the shock arrival that crossed all three EMIC wave bands. Strong ULF fluctuations in the Pc4–Pc5 frequency ranges and above were observed throughout the rest of the 13 November. Sometimes, these waves had harmonic structures that appeared consistent with ULF field line resonances.

A sudden increase in the intensity of the EMIC waves observed by GOES 15 near 14 LT was associated with the arrival of the shock at 2316 UT on 12 November. The strong wave activity observed by GOES 15 continued until about 0340 UT on 13 November, when GOES 15 was located near 18.5 LT. Before the shock arrival, the EMIC waves in the He^+ band at GOES 15 appeared most strongly in the parallel component of the

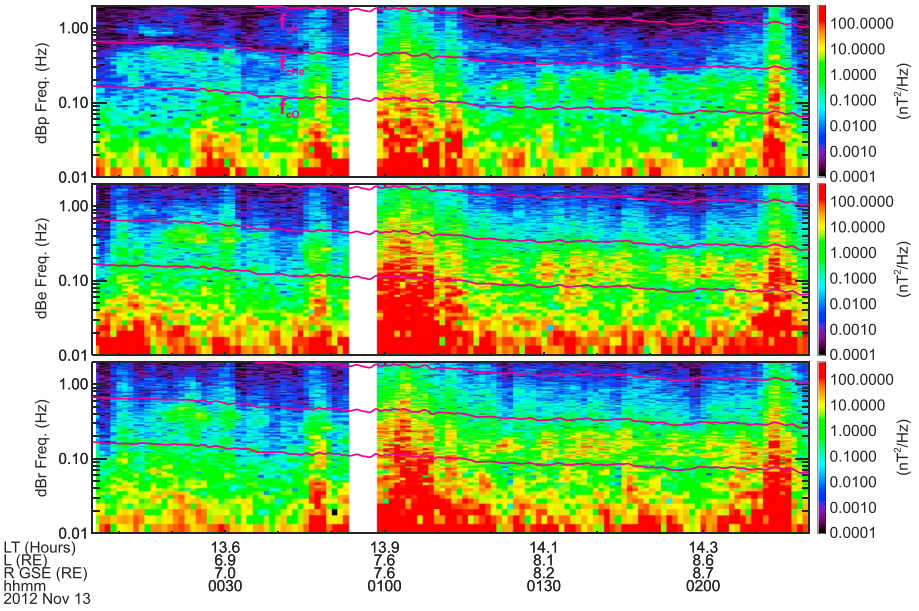

Figure 7. The THEMIS-A FGL magnetic field in field-aligned coordinates shortly after the shock arrival on 13 November 2012. Magenta lines for the O^+, He^+, and H^+ ion gyrofrequencies have been overplotted on the spectrograms.

magnetic field, with small bursts in the eastward and radial components. After the shock arrival, the EMIC waves at GOES 15 were most intense in the eastward component of the magnetic field. O^+ band waves may also have been observed, but they are difficult to separate from the strong ULF waves in the Pc4 and Pc5 bands that were also observed around the time of the shock arrival.

Although the shock arrival excited very strong EMIC waves on the dayside at GOES 15 near 14 LT, it only had a modest effect on the EMIC waves observed farther down the flanks of the magnetosphere by GOES 14 and GOES 13. A burst of slightly more intense EMIC waves was observed by GOES 14 near 17 LT around 2316 on 12 November and appears to be related to the shock arrival. Just like at GOES 15, the strongest fluctuations in the He^+ band at GOES 14 switched from mainly the parallel component before the shock arrival to the eastward component of the magnetic field after the shock arrival. Only a very slight increase in the EMIC wave intensity was observed by GOES 13 near 18 LT around the time of the shock arrival. Strong ULF waves in the Pc4–Pc5 frequency range were also observed by GOES 13 and 14.

Some of the ULF wave power observed by the Van Allen Probes in Figure 6 extended upward into the He^+ and H^+ EMIC wave frequency ranges at the time of the shock arrival and solar sector boundary crossing. However, much of the ULF wave power recorded by the Van Allen Probes throughout this event was due to waves at frequencies well below 1/10 of the O^+ cyclotron frequency. The character of the waves observed by the Van Allen Probes was not consistent with EMIC waves, as some wave bursts extended across all three EMIC wave bands and above the H^+ cyclotron frequency. The apogee of the Van Allen Probes was located near dawn, so it is not surprising that EMIC waves were not observed by the Van Allen Probes as statistical studies generally show that EMIC waves are observed most often near dusk [*Anderson et al.*, 1992a, 1992b]. It appears that EMIC waves were mainly observed outside the orbits of the Van Allen Probes during this event, consistent with studies showing that the occurrence rate of EMIC waves is low inside of geosynchronous orbit [*Usanova et al.*, 2012] and that dawnside EMIC waves tend to have smaller amplitudes and occur at larger radial distances than on the duskside [*Min et al.*, 2012]. Toroidal Pc4 and Pc5 field line resonances and harmonics continued to be observed in the eastward component of the magnetic field by the Van Allen Probes on 13 November.

Figure 7 shows the THEMIS-A Fluxgate Magnetometer low-resolution (FGL) [*Angelopoulos*, 2008; *Auster et al.*, 2008] magnetic field in field-aligned coordinates shortly after the shock arrival, from 0005 to 0230 UT on 13 November 2012. Only THEMIS slow survey data at 3 s resolution were available before 13 November 0000 UT, which do not have sufficient time resolution for studying He^+ and H^+ EMIC waves in this region. He^+ band

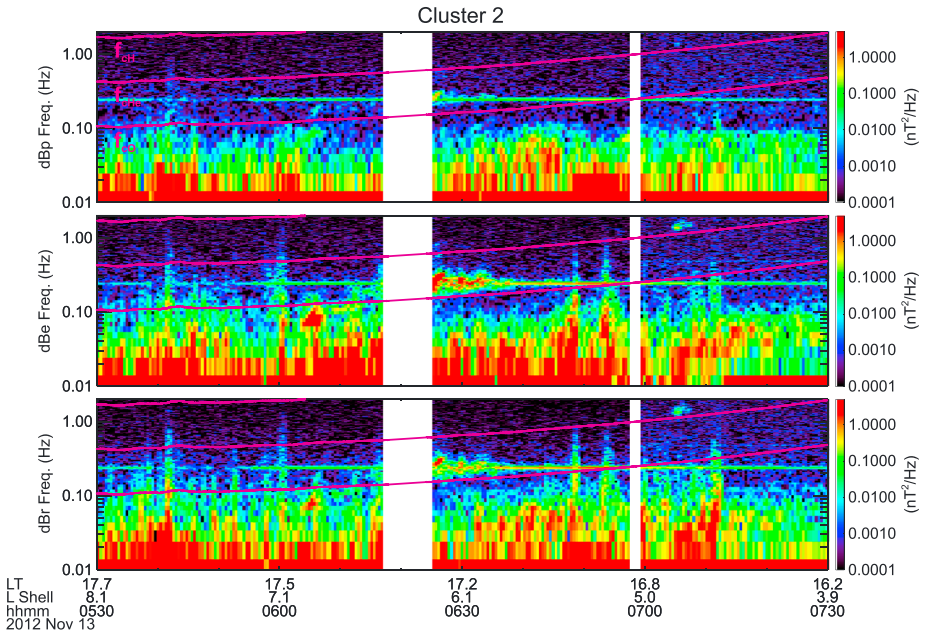

Figure 8. EMIC waves observed by the Cluster 2 FGM on 13 November around 0630 UT near 17 LT. The magnetic fields are in field-aligned coordinates.

EMIC waves are clearly seen in the THEMIS data, along with possible H^+ band waves. Lower frequency O^+ band waves may also be present but are difficult to separate from the strong ULF waves observed throughout the time period shown. The fluctuations observed by THEMIS-A are strongest in the perpendicular wave magnetic field components but also have a weaker parallel component. THEMIS-A observed these EMIC waves at radial distances between 6.3 and 9.1 R_E from 13.3 to 14.5 LT. The EMIC waves observed by THEMIS-A continue all the way out to the magnetopause on the dayside. The location of the THEMIS-A EMIC wave observations in the afternoon sector suggests the presence of a plasmaspheric plume, as EMIC waves have been associated with drainage plumes in the afternoon sector by past studies [*Morley et al.*, 2009; *Fraser et al.*, 2010; *Halford et al.*, 2015; *Yuan et al.*, 2012, 2013]. These waves may be generated by enhanced cold plasma densities within the plume [*Morley et al.*, 2009; *Halford et al.*, 2015]. Several hours of southward IMF occurred before the CME arrival and the observation of the EMIC waves by THEMIS-A, which is also consistent with the presence of a plume, as they are more likely to occur when convection is enhanced [e.g., *Walsh et al.*, 2013]. According to statistical analysis of THEMIS data presented by *Walsh et al.* [2013], the most common location where plumes contact the magnetopause is at 13.6 MLT. This is also consistent with the location of THEMIS-A during the event we studied.

After the main intervals of intense EMIC waves observed on 12–13 November by GOES 13 and 14 near dusk and by GOES 15 around the time of the sudden impulse, bursty waves in the EMIC frequency bands were recorded by all three GOES satellites and Cluster 2. Later in the day on 13 November, another short burst of EMIC waves was observed by GOES 14 from 0239 UT to 0305 UT between 20.7 and 21.2 LT and GOES 13 between 21.3 and 21.8 LT, possibly due to a sudden spike in the solar wind dynamic pressure near this time. Another burst of EMIC wave activity was observed between 13 November 0550 UT to 0715 UT by GOES 15 (21 LT) and GOES 14 (near 0.7 LT). Figure 8 shows EMIC waves observed by the Cluster 2 Fluxgate Magnetometer (FGM) [*Balogh et al.*, 2001] on 13 November between 0615 and 0640 UT near 17 LT. Note that in Figure 8, the Cluster spin period (4 s) is visible as a very narrow, flat line across the entire plot at 0.25 Hz. The bursty EMIC wave activity recorded by GOES 14, GOES 15, and Cluster 2 between 0550 UT and 0715 UT may have been associated with solar wind dynamic pressure fluctuations around this time, but there are no clear correlations between specific wave bursts and pressure variations.

To verify the identification of EMIC waves and to better understand the evolution of the EMIC wave properties before and after the shock arrival, the GOES 15 wave magnetic fields were analyzed with the PRopagation Analysis of STAFF-SA Data with COherency tests (PRASSADCO) software. PRASSADCO implements analysis methods to estimate the sense of polarization, ellipticity, and wave vector direction described, respectively,

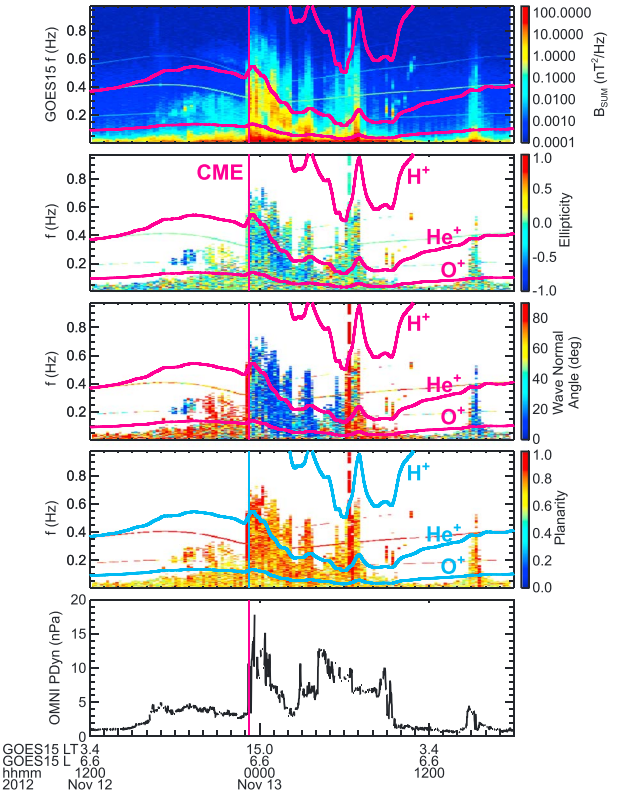

Figure 9. Results of wave normal analysis for GOES 15 on 12–13 November using PRASSADCO. From top to bottom are the total magnetic field power, the ellipticity, the wave normal angle, planarity, and solar wind dynamic pressure. Values of the ellipticity equal to −1 indicate left-hand polarization, +1 indicates right-hand polarization, and 0 indicates linear polarization. When the wave normal angle theta is 0°, the waves propagate parallel or antiparallel to the magnetic field, and when it is 90°, the waves propagate perpendicular to the magnetic field. The ellipticity, wave normal angle, and planarity are shown only for the total magnetic field power greater than 10^{-2} nT^2/Hz and planarity greater than 0.5. The ion cyclotron frequencies and CME arrival time have been marked on the plots.

by *Santolík et al.* [2001, 2002, 2003]. Because the GOES satellites do not have electric field data, we cannot determine Poynting vectors or resolve waves propagating antiparallel to one another as their magnetic fields will appear to be the same, but neither is important for wave identification. At frequencies below the proton cyclotron frequency, there are three possible wave modes: EMIC waves, magnetosonic waves, and Alfvén waves [*Gurnett and Bhattacharjee*, 2005]. Both Alfvén waves and magnetosonic waves are typically linearly polarized, but EMIC waves are normally left-hand polarized. There are reports in the literature (as discussed earlier) of linear and right-hand polarizations for EMIC waves, but those are not typical. Results from the analysis of 30 h of GOES 15 data from 1200 UT on 12 November to 1800 UT on 13 November with PRASSADCO are shown in Figure 9. As the PRASSADCO analysis assumes plane waves, the results can be poorly determined when the planarity is low. The ellipticity, wave normal angle, and planarity are therefore only plotted in Figure 9 when the wave power in the total magnetic field is greater than 10^{-2} nT^2/Hz and the planarity is greater than 0.5. These thresholds were used to analyze the most intense EMIC waves and ensure that Figure 9 only shows the ellipticity and wave normal angle when the PRASSADCO results are well determined. The ion cyclotron frequencies have been overplotted in Figure 9 with magenta lines on the spectrograms of the total magnetic field power, the ellipticity (−1 is left handed, 0 is linear, and +1 is right handed), and wave normal angle and in turquoise on the planarity. These colors were chosen for the frequencies to make them stand out from narrow instrumental lines due to the spacecraft heater that appear between 0.3 and 0.4 Hz and near 0.2 Hz. As can be seen in Figure 9, the He$^+$ EMIC band waves observed by GOES 15 on 12 November from 1600 UT up to the shock arrival at 2316 UT were mainly left handed (as indicated by the blue color) with large wave normal angles greater than 70°. However, the bursts of He$^+$ EMIC waves appearing in the eastward and radial components of the GOES 15 magnetic field between 1800 and 2000 UT were clearly left-hand polarized and had wave normal angles less than 30°, consistent with parallel propagation. The weak fluctuations in the H$^+$ EMIC band observed from around 2000 UT to 2316 UT were mostly left-hand polarized with some linearly polarized waves and large wave normal angles. These H$^+$ band waves do not appear in the wave normal analysis shown Figure 9 because they were below the 10^{-2} nT^2/Hz amplitude threshold chosen for this figure. GOES 15 was located between 7.3 LT and 14.3 LT when the nearly perpendicular propagating, left-hand to linearly polarized EMIC waves were observed, which is consistent with statistical studies showing that dawnside waves tend to be more linearly polarized and have large wave normal angles in the H$^+$ band (>45°) and even larger wave normal angles in the He$^+$ band (>60°) [e.g., *Anderson et al.*, 1992; *Min et al.*, 2012; *Allen et al.*, 2015].

The wave normal angle of the He^+ and H^+ band EMIC waves observed by GOES 15 abruptly drops to less than 20° when the CME shock arrives at 2316 UT on 12 November, indicating parallel propagation. The He^+ band waves now appear to be strongly left-hand polarized, while the H^+ band is left-hand to slightly linearly polarized. These conditions persist between 2316 UT on 12 November and 0600 UT on 13 November, when GOES 15 was located between 14.3 LT and 21.4 LT. This is consistent with statistical studies showing that duskside EMIC waves tend to be left-hand to linearly polarized and have smaller wave normal angles [*Anderson et al*., 1992a; *Min et al*., 2012]. Around 0600 UT on 13 November, the wave normal angles in both the He^+ and H^+ bands abruptly increase to values greater than 70° again, indicating perpendicular propagation. The polarizations after 0600 UT are mainly linear, with some left-hand polarized waves. Although the behavior of the EMIC waves during this event is similar to documented local time effects on EMIC wave properties, upstream solar wind conditions associated with the CME arrival also appear to have had an effect. Before the CME arrival, the IMF cone angle in Figure 1 was generally greater than 100°. From 2316 UT on 12 November to 0600 UT on 13 November, the IMF cone angle fluctuated, typically between values of 50° and 80°. After 0600 UT on 13 November, the IMF cone angle was consistently greater than 100° again. The intervals where the EMIC waves had nearly perpendicular propagation seem to roughly coincide with the intervals of higher IMF cone angles, while the parallel propagating waves occurred during lower IMF cone angles. EMIC waves observed in space tend to be very bursty and localized, similar to the short burst of waves observed by Cluster during this event shown in Figure 8. One of the most unique features of the EMIC waves observed by GOES 15 on 12–13 November was the extended duration of these waves over several hours UT and the broad range of magnetic local times on the dayside over which they were observed, as shown by Figures 2, 3, and 9.

The relativistic electron populations continued to evolve throughout 12–13 November in response to the ongoing EMIC wave activity, the arrival of the interplanetary shock, and further changes in the magnetic field configuration of the inner magnetosphere. The 2 MeV electron flux at GOES 13 and 14 remained flat at instrumental background levels, but the 2 MeV electron flux at GOES 15 continued decreasing from its peak value at 2054 UT on 12 November until 0103 UT on 13 November when it finally dropped to instrumental background levels. By the time of the sudden impulse at 2316 UT, the GOES 13 0.8 MeV electron flux had already dropped to less than 3% of its peak value at 1713 UT on 12 November and it continued to decrease, reaching a minimum value at 0239 UT on 13 November. By the time of the sudden impulse at 2316 UT, the GOES 14 0.8 MeV electron flux, which had also peaked at 1713 UT on 12 November, had dropped to about 5% of its maximum value. The GOES 14 0.8 MeV electron flux reached its minimum value at 0241 UT on 13 November, just 3 min later than GOES 13. At the time of the sudden impulse, the GOES 15 0.8 MeV electron flux had dropped only to 58% of its peak value on 12 November at 1950 UT, but it continued to decrease for several more hours on 13 November.

The Van Allen Probes provided information about both the spatial and temporal evolution of the electron fluxes [*Baker et al*., 2012; *Blake et al*., 2013] near the time of the shock arrival. Figure 10 shows the energetic electron fluxes observed by Van Allen Probe B (RBSP-B) for energies of 134 keV, 235 keV, 459 keV, 875 keV, 1040 keV, and 2 MeV as a function of time and *L* shell for the 72 h period from 0000 UT on 12 November to 0000 UT on 15 November. The 875 keV channel was selected because it was the closest in energy to the 0.8 MeV electrons measured by the GOES satellites. The electron data from Van Allen Probe A (RBSP-A) are similar to those shown in Figure 10. The electron flux dropout was first observed by the Van Allen Probes in the dawn magnetosphere after both spacecraft exited the plasmasphere and moved toward higher *L* shells around the time of the shock arrival.

Because Figure 10 shows that the electron flux dropout was more pronounced on the higher *L* shell portions of the Van Allen Probes orbits, we compared the electron fluxes with the location of the plasmapause to confirm that the apparent losses were not just due to the spacecraft leaving the plasmasphere. During the orbit (199 for RBSP-A and 198 for RBSP-B) just before the shock arrival on 12 November, the electron fluxes for energies close to 0.8 MeV and 2.0 MeV at both Van Allen Probes were well above instrumental background levels as the spacecraft reached apogee in the dawn magnetosphere. On the next orbit (200 for RBSP-A and 199 for RBSP-B), electron densities obtained from the upper hybrid line in the EMFISIS plasma wave [*Kurth et al*., 2015] data undergo a steep drop when both spacecraft crossed a sharp plasmapause boundary. RBSP-A observed the electron density drop by a factor of 130 between 2155 UT on 12 November when the spacecraft was located at $L = 4.2$ and 2.9 LT and 2221 UT when the spacecraft was located at $L = 4.8$ and 3.5 LT, just outside the plasmapause. For RBSP-B, the electron density dropped by a factor of 90 between 2219 UT on

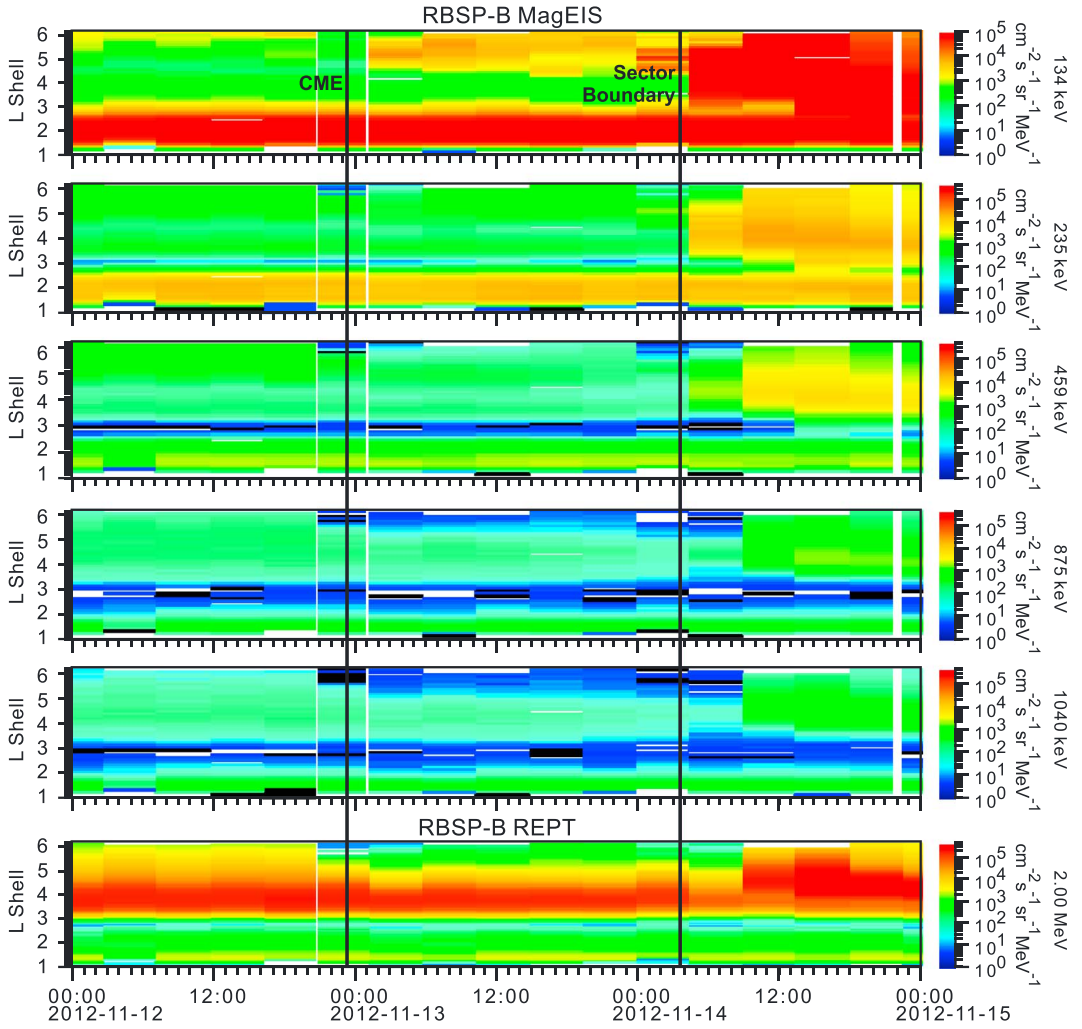

Figure 10. Magnetic Electron Ion Spectrometer (MagEIS) and REPT electron observations from Van Allen Probe B (RBSP-B) as a function of *L* shell and MLT for 12–14 November 2012. From top to bottom the energies are 134 keV, 235 keV, 459 keV, 875 keV, 1040 keV, and 2 MeV.

12 November when the spacecraft was located at $L = 4.0$ and 2.8 LT and 2259 UT when the spacecraft left the plasmasphere at $L = 4.9$ and 3.6 LT. The Van Allen Probes density measurements suggest that the plasmapause was located between about $L = 4$–5 in the local time region between 3.0 and 3.5 LT during this outbound crossing. The minimum density was measured by RBSP-A on this orbit at 2320 UT on 12 November when RBSP-A was located at $L = 5.8$ and 4.4 LT. The minimum density was measured by RBSP-B at 0054 UT on 13 November at $L = 6.2$ and 5.1 LT.

In the energy channel closest to 0.8 MeV measured by RBSP-A, a steep drop in the electron flux started at 2314 UT when the spacecraft was located at $L = 5.7$ and 4.3 LT. RBSP-B observed a steep drop in the 0.8 MeV electron flux starting at 2315 UT when the spacecraft was located at $L = 5.2$ and 3.8 LT. The 2.0 MeV electron flux observed by both RBSP-A and RBSP-B also began to drop rapidly to instrumental background levels at this time. According to the electron densities both RBSP-A and RBSP-B were already located outside the plasmapause when the electron fluxes began to decrease, indicating that the flux decreases observed by the Van Allen Probes for $L > 5$ in the dawnside magnetosphere were related to the shock arrival and were not simply due to the spacecraft exiting the plasmasphere.

As shown in Figure 10, a decrease in the Van Allen Probes electron fluxes was observed from 134 keV up to 2.0 MeV at the time of the shock arrival. Figure 10 shows that over the next few orbits, the 134 keV electron fluxes from $L \sim 4$ to 6 actually increased dramatically to levels greater than their values before the CME arrival and the

235 keV and 459 keV electrons quickly recovered from the decrease seen at the CME arrival. The 875 keV, 1040 keV, and 2.0 MeV electrons shown in Figure 10 increased slightly on the orbit after the CME arrival, but they remained at lower levels than before the CME arrival over the next several orbits for a period of time similar to the dropout in the 2 MeV electrons observed by GOES. The recovery of the lower energy electrons suggests that adiabatic processes may have played a role during this event, while the prolonged dropout in the higher energy electrons suggests that nonadiabatic processes also resulted in a permanent loss of some of the electron population.

The magnetic fields at GOES 13 and 14 remained stretched for several hours after the sudden impulse. The magnetic field inclination at GOES 13 began to rise after 0500 UT on 13 November, reaching a value of about 60° by 0650 UT, when GOES 13 was located at 2.2 LT. The GOES 14 inclination angle began to increase after the satellite passed through local midnight around 0540 UT on 13 November, reaching values above 60° around 0700 UT on 13 November when GOES 14 was located near 1.5 LT. While the stretched fields observed near dusk by GOES 13 and 14 may be due to formation of a partial ring current, enhanced solar wind convection probably contributed to the stretched fields observed by GOES 13 and 14 across the nightside. Although the magnetic field inclinations at GOES 13 and 14 had returned to more dipolar configurations by 0700 UT on 13 November, the 2 MeV electron fluxes at all three geosynchronous satellites remained at instrumental background levels. The 0.8 MeV electron fluxes begin increasing slowly after GOES 13 and 14 began observing more dipolar fields but continued to remain well below the peak fluxes observed on 12 November.

At the time of the shock arrival GOES 15 was located close to noon at 13.3 LT, and the magnetic field inclination actually increased slightly, from about 75° to 85° due to compression of the magnetosphere by the shock. The magnetic field inclination at GOES 15 remained above 70° until 0426 UT on 13 November, when GOES 15 was located near dusk at 19.7 LT and the magnetic field inclination started to decrease rapidly. The GOES 15 magnetic field inclination dropped to about 52° at 0522 UT when the satellite was located near 20.6 LT. At around 0600 UT, near 21.4 LT, the magnetic field inclination at GOES 15 jumped quickly to values above 70°, indicating possible propagation of a substorm dipolarization front past the spacecraft. After the dipolarization front passed, the magnetic field at GOES 15 became more taillike again and the inclination briefly dropped to about 40° at 0640 UT when the satellite was located near 22.1 LT. After about 0715 UT on 13 November, when GOES 15 was located near 22.7 LT, the GOES 15 inclination remained consistently above 60° throughout the rest of the day. Even though GOES 15 did not observe the extreme changes in magnetic field inclination that GOES 13 and 14 did, the 0.8 and 2.0 MeV fluxes at GOES 15 behaved in a similar manner to those at GOES 13 and 14.

The highly stretched magnetic fields observed by GOES 13 and 14 on 12–13 November suggest that the electron dropout was partially due to adiabatic effects. However, the behavior of the 0.8 MeV electrons at GOES 15 is similar to their behavior at GOES 13 and 14, even though GOES 15 never encounters the strongly tail-like magnetic fields observed by GOES 13 and 14. In spite of ongoing changes in the magnetic field configuration at geosynchronous orbit on 13 November, the 2 MeV electron fluxes at geosynchronous orbit remained at instrumental background levels until 14 November. The electron fluxes for the highest energies observed at the Van Allen Probes also remained at reduced levels throughout 13 November. This implies that in addition to adiabatic effects, there was also a permanent loss of electrons, likely due to the effects of the EMIC waves observed by GOES, THEMIS, and Cluster or losses to the magnetopause.

4. Solar Sector Boundary Crossing and the 13–14 November 2012 Electron Dropout

Throughout 13–14 November 2012, the solar wind speed remained elevated. Geomagnetic activity increased to major storm levels early on 14 November due to a prolonged period of negative IMF B_z related to the CMEs and a solar sector boundary crossing which reached Earth's bow shock on 14 November at 0336 UT. The solar sector boundary crossing was followed by a negative polarity coronal hole high-speed stream. Eventually, a storm developed with minimum *Dst* of about −100 nT at 0700 UT on 14 November.

The 2.0 MeV electron fluxes at GOES 13, 14, and 15 continued to remain at instrumental background levels throughout 13 November, even though the 0.8 MeV fluxes had recovered slightly by the end of the day. The 0.8 MeV flux reached peak values at GOES 13 at 2320 UT, GOES 14 at 2301 UT, and GOES 15 at 2258 UT. During the time period when the 0.8 MeV fluxes were recovering the magnetic field inclinations at GOES 13, 14 and 15 indicated that the satellites were in a region of highly dipolar fields. The recovery of the 0.8 MeV electron fluxes was likely related to a combination of the magnetic field configuration changes and acceleration by chorus and ULF waves which began to be observed by the Van Allen Probes after the shock arrival.

After the brief recovery, a second dropout in the 0.8 MeV electron fluxes at geosynchronous orbit occurred on 14 November as the geomagnetic storm developed and *Dst* decreased. The 134 keV, 235 keV, 459 keV, 875 keV, and 1040 keV electron fluxes on RBSP-B in Figure 10 also show another slight decrease around this time. At geosynchronous orbit, the development of this dropout appeared to be strongly correlated with the *Dst* index as shown by Figure 1 and with the magnetic field inclinations as shown by Figures 3, 4, and 5. As on 12–13 November, the 0.8 MeV flux decrease was also strongly correlated with the observation of stretched magnetic fields from dusk to dawn. During the 14 November dropout, the 0.8 MeV electron fluxes had a greater level of fluctuations than during the 13 November dropout. Brief fluctuations in the magnetic field inclination up to near 40° at GOES 14 on the nightside between 0045 and 0825 UT on 14 November may indicate a series of dipolarization fronts associated with substorm activity in the magnetotail. Similar fluctuations were observed by both GOES 14 and 15. The variations in the 0.8 MeV electron fluxes often appeared to be correlated with these fluctuations in the magnetic field inclination. After the passage of each dipolarization front, the magnetic field returned to a highly stretched configuration and the 0.8 MeV fluxes decreased again. As shown in Figure 1, the *Kp* index increased at the beginning of 14 November, possibly in response to the southward IMF. *Kp* remained elevated until noon, which appears consistent with the observation of substorm activity during the main phase of the storm.

The return of the electron fluxes to prestorm levels finally started as the *Dst* index began to increase and the magnetic field inclinations at geosynchronous orbit began increasing to a more dipolar configuration around 0900 UT. The change in magnetic field configuration was accompanied by increases in the 0.8 MeV and 2 MeV electron fluxes. The 0.8 MeV electron fluxes returned to their prestorm levels at GOES 13 at 1323 UT on 14 November and reached their maximum value for the day at 1548 UT. The GOES 13 2.0 MeV electron flux returned to its prestorm level several minutes later at 1338 UT on 14 November and continued to increase until reaching its maximum value for the day at 1548 UT, simultaneously with the 0.8 MeV electrons. For GOES 14, the return to the prestorm 0.8 MeV flux levels occurred at 1329 UT and the maximum value was reached at 1715 UT. The 2.0 MeV electron flux at GOES 14 returned to its prestorm value at 1344 UT on 14 November and reached its maximum value for the day at 1659 UT. At GOES 15, the 0.8 MeV fluxes returned to their prestorm value at 1332 UT and reached their peak value at 2116 UT. At GOES 15, the 2.0 MeV electron flux reached its prestorm value at 1350 UT on 14 November and reached its maximum value near the end of the day at 2115 UT.

On 14 November, bursty, low-frequency waves were observed by all three GOES satellites and the Van Allen Probes in association with an increase in the solar wind dynamic pressure at the beginning of the day, a few hours before the solar sector boundary crossing. These waves were broadband and did not feature the clear EMIC band structures that the waves observed by the GOES satellites on 12–13 November had. Analysis of the GOES 15 data with PRASSADCO shows that the waves observed on 14 November had mixed polarizations but were mainly linearly to right-hand polarized, with a very wide range of propagation directions. The absence of clear frequency bands and the PRASSADCO results suggest that these broadband ULF waves are not likely to be EMIC waves. The wave bursts observed by the Van Allen Probes were also broadband and extended across all three EMIC frequency bands and above the H^+ cyclotron frequency. As on 12 and 13 November, the ULF wave activity observed by the Van Allen Probes on 14 November did not appear to be consistent with EMIC waves because the most intense wave power was concentrated well below 1/10 of the O^+ cyclotron frequency and was within the Pc4–Pc5 frequency ranges. Harmonic structures typical of field line resonances can also be seen in the eastward component of the Van Allen Probes magnetic field on 14 November. Just before the end of 14 November, all three GOES satellites observed a strong Pc4 and Pc5 pulsations. This pulsation appeared in all three components of the magnetic field, but it was strongest in the parallel and radial components of the magnetic field, suggesting mainly compressional and poloidal pulsations. Compressional Pc5 pulsations are typically associated with storms and substorms [*Barfield and McPherron*, 1978; *Anderson*, 1994], while poloidal Pc4 and Pc5 pulsations are often observed during the recovery from prior geomagnetic activity [*Takahashi et al*., 1990; *Eriksson et al*., 2005, 2008; *Liu et al*., 2009] and are associated with plasmaspheric refilling [*Engebretson et al*., 1992]. Although these ULF waves do not appear to be associated with the electron losses, they likely contributed to the recovery of the energetic electrons at the end of the storm.

5. Discussion

The development of the initial electron flux dropout on 12–13 November at geosynchronous orbit occurred over time periods equivalent to many electron drift orbits. Although start time of the electron flux dropout varied

between spacecraft, the number of drift periods it took for the fluxes to reach their minimum value at both energies was similar at all three GOES spacecraft. For 2 MeV electrons, the bounce-averaged drift in a dipolar magnetic field [*Parks*, 1991] is about 5 min, and for 0.8 MeV electrons it is about 12 min. The 2 MeV electron flux at GOES 13 took 288 min or 58 drift periods to drop from the peak on 12 November at 1713 UT to below detectable levels. At GOES 14 it took 321 min (67 drift periods), and at GOES 15 it took 249 min (50 drift periods) to drop from the peak value at 2054 UT on 12 November to its lowest point at 0103 UT on 13 November. Although the 2 MeV flux at GOES 15 did not peak until nearly 3.75 h later than the 2 MeV flux at GOES 13 and 14, the number of drift periods for the electron fluxes at this energy to reach instrumental background levels at GOES 15 was similar to that at GOES 13 (60 drift periods) and GOES 14 (67 drift periods). For the 0.8 MeV electrons it took 566 min or about 47 drift periods from the peak in the GOES 13 electron at 1713 UT on 12 November to reach the minimum flux value at 0239 UT on 13 November. At GOES 15, the 0.8 MeV electron flux took 818 min or about 68 drift periods to reach its minimum value on 13 November at 0928 UT.

It is fairly typical for the development of electron dropout events to depend upon energy and local time [*Onsager et al*., 2002; *Green et al*., 2004]. In a study of 52 electron dropout events with rapid decreases in the $>$2 MeV electron fluxes at geosynchronous orbit, the events typically began in the dusk sector, simultaneously with the stretching of the magnetic field caused by the formation of a partial ring current driven by upstream solar wind conditions [*Green et al*., 2004]. As the discussion in the previous paragraph indicates, the event studied here follows this pattern, because GOES 13, which was located the closest to dusk of all three GOES spacecraft on 12 November at the start of the dropout, observed the start of the electron flux dropout well before GOES 15, which was located farthest away from dusk of the three geosynchronous satellites at the start of the dropout. The Van Allen Probes, which had apogee near dawn around the time of the shock arrival on 12 November, were the last to observe the dropout. It is also interesting to note that during the start of the first interval of reduced 0.8 MeV electron fluxes on 12–13 November, the degree of stretching indicated by the magnetic field inclination at GOES 15 was much less than those at GOES 13 and 14. However, all three geosynchronous satellites observed a similar degree of stretching on 14 November during the second interval of decreased 0.8 MeV electron fluxes. GOES 15 was near similar local times at the start of both intervals of reduced 0.8 MeV electron fluxes. The differences in the responses of the magnetic field and electrons at GOES 15 may be due to both the differences in the solar wind drivers and state of the magnetosphere during these two time periods.

As shown by Figures 1, 3, 4, and 5, the initial phase of the electron flux dropout on 12–13 November does not appear to be the result of the *Dst* effect. There could be a correlation between the decrease in the 2 MeV electron fluxes at GOES 13 and 14 at the start of the dropout on 12 November and a slight decrease in the *Dst* index around the same time, but no correlation is seen with the 2 MeV electrons at GOES 15. The 2 MeV electrons at all three GOES satellites quickly reached instrumental background levels on 12–13 November and remained at that level until *Dst* begins to recover near the end of the day on 14 November. The behavior of the 0.8 MeV electrons at GOES 13, 14, and 15 also does not appear to track the *Dst* index throughout 12 November and most of 13 November and instead appears to be better correlated with stretching of the magnetic field. In the early afternoon on 13 November, the GOES 13, 14, and 15 0.8 MeV electron fluxes actually begin to recover, while the *Dst* index has a gradual decreasing trend. However, the second phase of the 0.8 MeV electron flux decrease, which starts at the end of 13 November, definitely follows the *Dst* index as it drops steadily to values below -100 nT on 14 November. Both the 0.8 MeV and 2 MeV electron fluxes at all three GOES satellites begin to recover as *Dst* increases, but the 2 MeV electron fluxes take longer to increase. This may be because the dropout in the 0.8 MeV electrons on 13–14 November was caused mainly by adiabatic processes, so that the electrons recovered quickly in response to magnetic field configuration changes at the end of the storm. The prolonged decrease in the 2 MeV fluxes from 12 to 14 November appears to have represented a permanent loss of electrons, and thus, the 2 MeV fluxes required the acceleration of lower energy electrons to fully recover.

Although the GOES satellites did not observe any magnetopause crossings at geosynchronous orbit during this event, there were strong variations in the solar wind dynamic pressure and intervals of southward IMF during the time period of interest. Such variations in upstream conditions have been associated with permanent losses to the magnetopause by recent studies [e.g., *Kim et al*., 2008, 2010; *Matsumura et al*., 2011; *Yu et al*., 2011]. As noted by *Matsumura et al*. [2011], if geosynchronous satellites are the farthest satellites from Earth used in a study, the outermost edge of the radiation belt associated with electron losses to the

magnetopause might not be detected. As a result, we cannot rule out possible contributions by magnetopause shadowing to the electron flux dropout event studied in this paper, particularly on 12–13 November, when the greatest solar wind dynamic pressure variations were observed.

Examining the THEMIS, Cluster, and GOES locations on 12–13 November, we see that EMIC waves were observed mainly in the afternoon and dusk sectors at geosynchronous orbit and beyond, over a region of several hours in local time and 2–4 R_E wide. The Van Allen Probes appeared to have been located too far inside the magnetosphere to see this EMIC wave activity. The local time of the Van Allen Probes apogee near dawn during this event may have been a factor in the wave observations, as EMIC waves are typically thought of as being strongest at dusk. The observed region of EMIC wave occurrence during this event is consistent with statistical studies [*Anderson et al*., 1992a, 1992b; *Usanova et al*., 2012; *Min et al*., 2012; *Meredith et al*., 2014]. Electron fluxes at geosynchronous orbit were already beginning to decrease on 12 November 2012, in association with the EMIC waves, before the shock arrival at 2316 UT. This suggests that the magnetosphere was already primed for the development of a deep electron dropout by preexisting EMIC waves at the time of the shock arrival. In Figures 2 and 3, the occurrence of the EMIC waves at geosynchronous orbit appears well correlated with the development of the initial electron flux dropout at 0.8 MeV on 12–13 November, but as the previous discussion shows it is likely that the variations in the 0.8 MeV electrons at GOES and the 235 keV and 459 keV electrons at the Van Allen Probes were mainly caused by reversible changes in the magnetic field configuration. The prolonged dropout in the 2.0 MeV electrons indicates that a permanent loss of electrons developed over time scales of a few hours, which is consistent with the time scales for scattering by EMIC waves [*Summers et al*., 2007].

The observations during this event are somewhat different from other recent studies of electron flux dropouts, which concluded that magnetopause shadowing is an important loss mechanism for values of L or $L^* > 5$ and that other processes, such as wave-particle interactions with EMIC waves, may be more important for $L < 5$ [e.g., *Bortnik et al*., 2006; *Yu et al*., 2013]. In the event studied here, there was little variation in the electron fluxes for $L < 5$ and the losses of relativistic electrons for $L > 5$ may have resulted from a combination of wave-particle interactions, changes to the magnetic field configuration, and magnetopause shadowing.

6. Conclusions

We conclude that the initial phase of the electron dropout observed by GOES 13, 14, and 15 and the Van Allen Probes on 12–13 November 2012 was caused by a combination of adiabatic processes due to local stretching of the magnetic field near dusk, along with nonadiabatic processes due to wave-particle interactions with the He^+ EMIC waves observed by THEMIS, Cluster, and the three GOES satellites. Although no magnetopause crossings were observed at geosynchronous orbit, we cannot rule out that magnetopause shadowing may have played a role in the observed electron behavior during this event, due to the enhanced solar wind dynamic pressure and the arrival of the CME on 12 November. After noon on 13 November, the greater than 2 MeV electron fluxes remained at instrumental background levels, while the lower energy electron fluxes recovered slightly. This brief recovery in the 0.8 MeV electrons at geosynchronous orbit may have been caused by electron acceleration processes associated with ULF waves and chorus observed by the Van Allen Probes, as well as changes in the magnetic field configuration of the inner magnetosphere. The second phase of the dropout in the 0.8 MeV electrons on 13–14 November 2012 appears to be mainly due to adiabatic processes such as magnetic field stretching and the *Dst* effect in response to upstream solar wind drivers. As the *Dst* index began to increase at the start of the storm recovery phase on 14 November, the particle fluxes gradually increased to prestorm values.

Acknowledgments

This work was performed under JHU/APL contract 921647 under NASA prime contract NAS5-01072. We acknowledge William Kurth for providing density calculations from the EMFISIS data. RBSP-ECT funding was provided by JHU/APL contract 967399 under NASA prime contract NAS5-01072. O. Santolík acknowledges funding from the Czech Academy of Sciences through the Praemium Academiae award and from the LH14010 grant. We acknowledge NASA contract NAS5-02099 and V. Angelopoulos for use of data from the THEMIS Mission. Specifically, K.H. Glassmeier, U. Auster, and W. Baumjohann provided THEMIS FGM data under the lead of the Technical University of Braunschweig and with financial support through the German Ministry for Economy and Technology and the German Center for Aviation and Space (DLR) under contract 50 OC 0302. Data from the Van Allen Probes can be obtained through the Van Allen Probes Science Gateway (http://rbspgway.jhuapl.edu/). GOES data are available from the NOAA National Geophysical Data Center, and the Preliminary Reports and Forecasts of Solar Geophysical Data are available from the NOAA Space Weather Prediction Center. THEMIS data are publicly available through the University of California Berkeley (http://themis.ssl.berkeley.edu). Cluster data are available from the Cluster Science Archive. Solar wind data and geomagnetic indexes are available online from NASA OMNIWeb. Wind and ACE data are available online through CDAWeb.

References

Allen, R. C., J.-C. Zhang, L. M. Kistler, H. E. Spence, R.-L. Lin, B. Klecker, M. W. Dunlop, M. André, and V. K. Jordanova (2015), A statistical study of EMIC waves observed by Cluster 1: Wave properties, *J. Geophys. Res. Space Physics*, *120*, 5574–5592, doi:10.1002/2015JA021333.

Anderson, B. J. (1994), An overview of spacecraft observations of 10 s to 600 s period magnetic pulsations in the Earth's magnetosphere, in *Solar Wind Sources of Magnetospheric Ultra-Low-Frequency Waves*, *Geophys. Monogr. Ser.*, vol. 81, edited by M. J. Engebretson, K. Takahashi, and M. Scholer, pp. 25–43, AGU, Washington, D. C., doi:10.1029/GM081p0025.

Anderson, B., R. Erlandson, and L. Zanetti (1992a), A statistical study of Pc 1–2 magnetic pulsations in the equatorial magnetosphere: 2. Wave properties, *J. Geophys. Res.*, *97*, 3089–3101, doi:10.1029/91JA02697.

Anderson, B., R. Erlandson, and L. Zanetti (1992b), A statistical study f Pc 1–2 magnetic pulsations in the equatorial magnetosphere: 1. Equatorial occurrence distributions, *J. Geophys. Res.*, *97*, 3075–3088, doi:10.1029/91JA02706.

Angelopoulos, V. (2008), The THEMIS Mission, *Space Sci. Rev.*, *141*, 5–34, doi:10.1007/s11214-008-9336-1.
Auster, H. U., et al. (2008), The THEMIS Fluxgate Magnetometer, *Space Sci. Rev.*, *141*, 235–264, doi:10.1007/s11214-008-9365-9.
Baker, D. N., et al. (2012), The Relativistic Electron-Proton Telescope (REPT) instrument on board the Radiation Belt Storm Probes (RBSP) spacecraft: Characterization of Earth's radiation belt high-energy particle populations, *Space Sci. Rev.*, *179*, 337–381, doi:10.1007/s11214-012-9950-9.
Balogh, A., et al. (2001), The Cluster magnetic field investigation: Overview of in-flight performance and initial results, *Ann. Geophys.*, *19*, 1207–1217, doi:10.5194/angeo-19-1207-2001.
Barfield, J. N., and R. L. McPherron (1978), Stormtime Pc 5 magnetic pulsations observed at synchronous orbit and their correlation with the partial ring current, *J. Geophys. Res.*, *83*, 739–743, doi:10.1029/JA083iA02p00739.
Blake, J. B., et al. (2013), The Magnetic Electron Ion Spectrometer (MagEIS) instruments aboard the Radiation Belt Storm Probes (RBSP) spacecraft, *Space Sci. Rev.*, *179*, 383–421, doi:10.1007/s11214-013-9991-8.
Bortnik, J., R. M. Thorne, T. P. O'Brien, J. C. Green, R. J. Strangeway, Y. Y. Shprits, and D. N. Baker (2006), Observation of two distinct, rapid loss mechanisms during the 20 November 2003 radiation belt dropout event, *J. Geophys. Res.*, *111*, A12216, doi:10.1029/2006JA011802.
Bräysy, T., K. Mursula, and G. Marklund (1998), Ion cyclotron waves during a great magnetic storm observed by Freja double-probe electric field instrument, *J. Geophys. Res.*, *103*, 4145–4155, doi:10.1029/97JA02820.
Brueckner, G. E., et al. (1995), The Large Angle Spectroscopic Coronagraph (LASCO), *Sol. Phys.*, *162*, 357–402.
Engebretson, M. J., D. L. Murr, K. N. Erickson, R. J. Strangeway, D. M. Klumpar, S. A. Fuselier, L. J. Zanetti, and T. A. Potemra (1992), The spatial extent of radial magnetic pulsation events observed in the dayside near synchronous orbit, *J. Geophys. Res.*, *97*, 13,741–13,758, doi:10.1029/92JA00992.
Eriksson, P. T. I., L. G. Blomberg, A. D. M. Walker, and K.-H. Glassmeier (2005), Poloidal ULF oscillations in the dayside magnetosphere: A Cluster study, *Ann. Geophys.*, *23*, 2679–2686, doi:10.5194/angeo-23-2679-2005.
Eriksson, P. T. I., L. G. Blomberg, S. Schaefer, and K. -H. Glassmeier (2008), Sunward propagating Pc5 waves observed on the post-midnight magnetospheric flank, *Ann. Geophys.*, *26*, 1567–1579, doi:10.5194/angeo-26-1567-2008.
Fraser, B. J., R. S. Grew, S. K. Morley, J. C. Green, H. J. Singer, T. M. Loto'aniu, and M. F. Thomsen (2010), Storm time observations of electromagnetic ion cyclotron waves at geosynchronous orbit: GOES results, *J. Geophys. Res.*, *115*, A05208, doi:10.1029/2009JA014516.
Green, J. C., T. G. Onsager, T. P. O'Brien, and D. N. Baker (2004), Testing loss mechanisms capable of rapidly depleting relativistic electron flux in the Earth's outer radiation belt, *J. Geophys. Res.*, *109*, A12211, doi:10.1029/2004JA010579.
Gurnett, D. A., and A. Bhattacharjee (2005), *Introduction to Plasma Physics with Space and Laboratory Applications*, Cambridge Univ. Press, New York.
Halford, A., B. J. Fraser, and S. K. Morley (2015), EMIC waves and plasmaspheric plume density: CRRES results, *J. Geophys. Res. Space Physics*, *120*, 1974–1992, doi:10.1002/2014JA020338.
Howard, R. A., et al. (2008), Sun Earth Connection Coronal and Heliospheric Investigation (SECCHI), *Space Sci. Rev.*, *136*, 67–115, doi:10.1007/s11214-008-9341-4.
Hughes, J. W. (1994), Magnetospheric ULF waves: A tutorial with a historical perspective, in *Solar Wind Sources of Magnetospheric Ultra-Low-Frequency Waves*, *Geophys. Monogr. Ser.*, vol. 81, edited by M. J. Engebretson, K. Takahashi, and M. Scholer, pp. 1–11, AGU, Washington, D. C., doi:10.1029/GM081p0001.
Jacobs, J. A., Y. Kato, S. Matsushita, and V. A. Troitskaya (1964), Classification of geomagnetic micropulsations, *J. Geophys. Res.*, *69*, 180–181, doi:10.1029/JZ069i001p00180.
Kim, H.-J., and A. A. Chan (1997), Fully adiabatic changes in storm time relativistic electron fluxes, *J. Geophys. Res.*, *102*, 22,107–22,116, doi:10.1029/97JA01814.
Kim, K. C., D.-Y. Lee, H.-J. Kim, L. R. Lyons, E. S. Lee, M. K. Öztürk, and C. R. Choi (2008), Numerical calculations of relativistic electron drift loss effect, *J. Geophys. Res.*, *113*, A09212, doi:10.1029/2007JA013011.
Kim, K. C., D.-Y. Lee, H.-J. Kim, E. S. Lee, and C. R. Choi (2010), Numerical estimates of drift loss and Dst effect for outer radiation belt relativistic electrons with arbitrary pitch angle, *J. Geophys. Res.*, *115*, A03028, doi:10.1029/2009JA014523.
King, J. H., and N. E. Papitashvili (2005), Solar wind spatial scales in and comparisons of hourly Wind and ACE plasma and magnetic field data, *J. Geophys. Res.*, *110*, A02104, doi:10.1029/2004JA010649.
Kletzing, C. A., et al. (2013), The Electric and Magnetic Field Instrument Suite and Integrated Science (EMFISIS) on RBSP, *Space Sci. Rev.*, *179*, 127–181, doi:10.1007/s11214-013-9993-6.
Kozyra, J., T. Cravens, A. Nagy, E. Fontheim, and R. Ong (1984), Effects of energetic heavy ions on electromagnetic ion cyclotron wave generation in the plasmapause region, *J. Geophys. Res.*, *89*, 2217–2233, doi:10.1029/JA089iA04p02217.
Kurth, W. S., S. De Pascuale, J. B. Faden, C. A. Kletzing, G. B. Hospodarsky, S. Thaller, and J. R. Wygant (2015), Electron densities inferred from plasma wave spectra obtained by the Waves instrument on Van Allen Probes, *J. Geophys. Res. Space Physics*, *120*, 904–914, doi:10.1002/2014JA020857.
Li, X., D. N. Baker, M. Temerin, T. E. Cayton, E. G. D. Reeves, R. A. Christensen, J. B. Blake, M. D. Looper, R. Nakamura, and S. G. Kanekal (1997), Multisatellite observations of the outer zone electron variation during the November 3–4, 1993, magnetic storm, *J. Geophys. Res.*, *102*, 14,123–14,140, doi:10.1029/97JA01101.
Liu, W., T. E. Sarris, X. Li, S. R. Elkington, R. Ergun, V. Angelopoulos, J. Bonnell, and K. H. Glassemeier (2009), Electric and magnetic field observations of Pc4 and Pc5 pulsations in the inner magnetosphere: A statistical study, *J. Geophys. Res.*, *114*, A12206, doi:10.1029/2009JA014243.
Lopez, R. E., A. T. Y. Lui, D. G. Sibeck, R. W. McEntire, L. J. Zanetti, T. A. Potemra, and S. M. Krimigis (1988), The longitudinal and radial distribution of magnetic reconfigurations in the near-Earth magnetotail as observed by AMTE/CCE, *J. Geophys. Res.*, *93*, 997–1001, doi:10.1029/JA093iA02p00997.
Matsumura, C., Y. Miyoshi, K. Seki, S. Saito, V. Angelopoulos, and J. Koller (2011), Outer radiation belt boundary location relative to the magnetopause: Implications for magnetopause shadowing, *J. Geophys. Res.*, *116*, A06212, doi:10.1029/2011JA016575.
Meredith, N. P., R. M. Thorne, R. B. Horne, D. Summers, B. J. Fraser, and R. R. Anderson (2003), Statistical analysis of relativistic electron energies for cyclotron resonance with EMIC waves observed on CRRES, *J. Geophys. Res.*, *108*(A6), 1250, doi:10.1029/2002JA009700.
Meredith, N. P., R. B. Horne, T. Kersten, B. J. Fraser, and R. S. Grew (2014), Global morphology and spectral properties of EMIC waves derived from CRRES observations, *J. Geophys. Res. Space Physics*, *119*, 5328–5342, doi:10.1002/2014JA020064.
Millan, R. M., and R. M. Thorne (2007), Review of radiation belt relativistic electron losses, *J. Atmos. Sol. Terr. Phys.*, *69*, 362–377, doi:10.1016/j.jastp.2006.06.019.
Min, K., J. Lee, K. Keika, and W. Li (2012), Global distribution of EMIC waves derived from THEMIS observations, *J. Geophys. Res.*, *117*, A05219, doi:10.1029/2012JA017515.
Morley, S. K., S. T. Ables, M. D. Sciffer, and B. J. Fraser (2009), Multipoint observations of Pc1-2 waves in the afternoon sector, *J. Geophys. Res.*, *114*, A09205, doi:10.1029/2009JA014162.

Morley, S. K., R. H. W. Friedel, E. L. Spanswick, G. D. Reeves, J. T. Steinberg, J. Koller, T. E. Cayton, and E. Noveroske (2010), Dropouts of the outer electron radiation belt in response to solar wind stream interfaces: Global positioning system observations, *Proc. R. Soc. A.*, *466*, 3329–3350, doi:10.1098/rspa.2010.0078.

Onsager, T. G., G. Rostoker, H.-J. Kim, G. D. Reeves, T. Obara, H. J. Singer, and C. Smithro (2002), Radiation belt electron flux dropouts: Local time, radial, and particle-energy dependence, *J. Geophys. Res.*, *107*(A11), 1382, doi:10.1029/2001JA000187.

Parks, G. K. (1991), *Physics of Space Plasmas*, Addison-Wesley Comp., New York.

Paulson, K. W., C. W. Smith, M. R. Lessard, M. J. Engebretsen, R. B. Torbert, and C. A. Kletzing (2014), In situ observations of Pc1 pearl pulsations by the Van Allen Probes, *Geophys. Res. Lett.*, *41*, 1823–1829, doi:10.1002/2013GL059187.

Reeves, G. D. (1998), Relativistic electrons and magnetic storms: 1992–1995, *Geophys. Res. Lett.*, *25*, 1817–1820, doi:10.1029/98GL01398.

Reeves, G. D., K. L. McAdams, R. H. W. Friedel, and T. P. O'Brien (2003), Acceleration and loss of relativistic electrons during geomagnetic storms, *Geophys. Res. Lett.*, *30*(10), 1529, doi:10.1029/2002GL016513.

Santolík, O., E. Lefeuvre, M. Parrot, and J. L. Rauch (2001), Complete wave-vector directions of electromagnetic emissions: Application to INTERBALL-2 measurements in the nightside auroral zone, *J. Geophys. Res.*, *106*, 13,191–13,201, doi:10.1029/2000JA000275.

Santolík, O., J. S. Pickett, D. A. Gurnett, and L. R. O. Storey (2002), Magnetic component of narrowband ion cyclotron waves in the auroral zone, *J. Geophys. Res.*, *107*(A12), 1444, doi:10.1029/2001JA000146.

Santolík, O., M. Parrot, F. Lefeuvre (2003) Singular value decomposition methods for wave propagation analysis, *Radio Sci.*, *38*(1), 1010, doi:10.1029/2000RS002523.

Sigsbee, K., J. A. Slavin, R. P. Lepping, A. Szabo, M. Øieroset, M. L. Kaiser, M. J. Reiner, and H. J. Singer (2005), Statistical and superposed epoch study of dipolarization events using data from Wind perigee passes, *Ann. Geophys.*, *23*, 831–851, doi:10.5194/angeo-23-831-2005.

Summers, D., B. Ni, and N. P. Meredith (2007), Timescales for radiation belt electron acceleration and loss due to resonant wave-particle interactions: 2. Evaluation for VLF chorus, ELF hiss, and electromagnetic ion cyclotron waves, *J. Geophys. Res.*, *112*, A04207, doi:10.1029/2006JA011993.

Takahashi, K., R. W. McEntire, A. T. Y. Lui, and T. A. Potemra (1990), Ion flux oscillations associated with a radially polarized transverse Pc 5 magnetic pulsation, *J. Geophys. Res.*, *95*, 3717–3731, doi:10.1029/JA095iA04p03717.

Takahashi, K., R. E. Denton, W. Kurth, C. Kletzing, J. Wygant, J. Bonnell, L. Dai, K. Min, C. W. Smith, and R. MacDowell (2015), Externally driven plasmaspheric ULF waves observed by the Van Allen Probes, *J. Geophys. Res. Space Physics*, *120*, 526–522, doi:10.1002/2014JA020373.

Thorne, R., and C. Kennel (1971), Relativistic electron precipitation during magnetic storm main phase, *J. Geophys. Res.*, *76*, 4446–4453, doi:10.1029/JA076i019p04446.

Thorne, R., and R. Horne (1994), Energy transfer between energetic ring current H+ and O+ by electromagnetic ion cyclotron waves, *J. Geophys. Res.*, *99*, 17,275–17,282, doi:10.1029/94JA01007.

Turner, D. L., Y. Shprits, M. Hartinger, and V. Angelopoulos (2012), Explaining sudden losses of outer radiation belt electrons during geomagnetic storms, *Nat. Phys.*, *8*, 208–212, doi:10.1038/NPHS2185.

Turner, D. L., S. K. Morley, Y. Miyoshi, B. Ni, and C.-L. Huang (2013), Outer radiation belt flux dropouts: Current understanding and unresolved questions, in *Dynamics of the Earth's Radiation Belts and Inner Magnetosphere*, *Geophys. Monogr. Ser.*, vol. 199, edited by D. Summers, et al., pp. 195–212, AGU, Washington D. C, doi:10.1029/2012GM001310.

Usanova, M. E., I. R. Mann, J. Bortnik, L. Shao, and V. Angelopoulos (2012), THEMIS observations of electromagnetic ion cyclotron wave occurrence: Dependence on AE, SYMH, and solar wind dynamic pressure, *J. Geophys. Res.*, *117*, A10218, doi:10.1029/2012JA018049.

Walsh, B. M., D. G. Sibeck, Y. Nishimura, and V. Angelopoulos (2013), Statistical analysis of the plasmaspheric plume at the magnetopause, *J. Geophys. Res. Space Physics*, *118*, 4844–4851, doi:10.1002/jgra.50458.

West, H. I., R. M. Buck, and J. R. Walton (1972), Shadowing of electron azimuthal-drift motions near the noon magnetopause, *Nat. Phys. Sci.*, *240*, 6–7, doi:10.1038/physci240006a0.

Yu, Y., J. Koller, and S. K. Morley (2013), Quantifying the effect of magnetopause shadowing on electron radiation belt dropouts, *Ann. Geophys.*, *31*, 1929–1939, doi:10.5194/angeo-31-1929-2013.

Yuan, Z., X. Deng, X. Lin, Y. Peng, M. Zhou, P. M. E. Décréau, J. G. Trotignon, E. Lucek, H. U. Frey, and J. Wang (2012), Link between EMIC waves in plasmaspheric plume and a detached sub-auroral proton arc with observations of Cluster and IMAGE satellites, *Geophys. Res. Lett.*, *37*, L07108, doi:10.1029/2010GL042711.

Yuan, Z., M. Li, Y. Xiong, H. Li, M. Zhou, D. Wang, S. Huang, X. Deng, and J. Wang (2013), Simultaneous observations of precipitating radiation belt electrons and ring current ions associated with the plasmaspheric plume, *J. Geophys. Res. Space Physics*, *118*, 4391–4399, doi:10.1002/jgra.50432.